International Journal of Nanomedicine

Dovepress

open access to scientific and medical research

Open Access Full Text Article

ORIGINAL RESEARCH

High-affinity carboxyl-graphene oxide-based SPR aptasensor for the detection of hCG protein in clinical serum samples

This article was published in the following Dove Press journal:
International Journal of Nanomedicine

Nan-Fu Chiu[1]
Chia-Tzu Kuo[1]
Chen-Yu Chen[2,3]

[1]Laboratory of Nano-Photonics and Biosensors, Institute of Electro-Optical Engineering, National Taiwan Normal University, Taipei 11677, Taiwan; [2]Department of Obstetrics and Gynecology, Mackay Memorial Hospital, Taipei City 10449, Taiwan; [3]Department of Medicine, Mackay Medical College, Taipei 252, Taiwan

Background: The use of functionalized graphene oxide (fGO) has led to a new trend in the sensor field, owing to its high sensitivity with regards to sensing characteristics and easy synthesis procedures.

Methods: In this study, we developed an ultra-sensitive carboxyl-graphene oxide (carboxyl-GO)-based surface plasmon resonance (SPR) aptasensor using peptides to detect human chorionic gonadotropin (hCG) in clinical serum samples. The carboxyl-GO based SPR aptasensor provided high affinity and stronger binding of peptides, which are great importance to allow for a non-immunological label-free mechanism. Also, it allows the detection of low concentrations of hCG, which are in turn considered to be important clinical parameters to diagnose ectopic pregnancies and paraneoplastic syndromes.

Results: The high selectivity of the carboxyl-GO-based SPR aptasensor for hCG recombinant protein was verified by the addition of the interfering proteins bovine serum albumin (BSA) and human serum albumin (HSA), which did not affect the sensitivity of the sensor. The carboxyl-GO-based chip can enhance the assay efficacy of interactions between peptides and had a high affinity binding for a k_a of 17×10^6 $M^{-1}S^{-1}$. The limit of detection for hCG in clinical serum samples was 1.15 pg/mL

Conclusion: The results of this study demonstrated that the carboxyl-GO-based SPR aptasensor had excellent sensitivity, affinity and selectivity, and thus the potential to be used as disease-related biomarker assay to allow for an early diagnosis, and possibly a new area in the field of biochemical sensing technology.

Keywords: carboxyl-graphene oxide (carboxyl-GO), surface plasmon resonance (SPR), human chorionic gonadotropin (hCG)

Introduction

Graphene is an advanced two-dimensional (2D) layered material with unique and excellent mechanical, electrical and optical properties such as high tensile strength,[1,2] high conductivity,[2,3] and high transmittance.[4] Its structure on the atomic-scale is a hexagonal allotrope of carbon. In addition, it has the same properties as the derivatives of graphene-based materials such as graphene oxide (GO) and reduced graphene oxide (rGO) sheets. Controlling the oxygen content in the oxygen functional groups on the surface of GO sheets can improve biological affinity,[5–7] modulate plasmonics,[8] change the electrical conductivity characteristics,[9] and modulate the band-gap to change the luminescence wavelength shift,[8,10] allowing for excellent modulation mechanisms. Therefore, GO represents a highly modifiable and malleable carbon-based functional

Correspondence: Nan-Fu Chiu
Laboratory of Nano-photonics and Biosensors, Institute of Electro-Optical Engineering, National Taiwan Normal University, No. 88, Sec. 4, Ting-Chou Road, Taipei 11677, Taiwan
Tel +88 627 734 6722
Fax +88 628 663 1954
Email nfchiu@ntnu.edu.tw

submit your manuscript | www.dovepress.com
DovePress
http://doi.org/10.2147/IJN.S208292

material with almost unlimited potential which can be inexpensively produced. It has been extensively studied and successfully used in the development of biosensor,[5,11–13] and optoelectronic devices.[8]

The structure and functionalization properties of GO with regards to peptides has gained increasing interest with regards to its use as a biosensor. Owing to the ability of GO sheets to specifically bind to a given target biomolecule, they allow for a new experimental strategy for functional peptide analysis. In addition, the application of GO-based biosensor technology in biological sensing devices has rapidly increased in a wide variety of diagnostic fields including genetic diseases and cancer, in order to identify proteomes and new drugs. Our previous study successfully demonstrated the interactions between GO and proteins,[5] the development of GO for immunoassays,[13] and the determination of GO-peptide interactions.[14] Compared with a conventional bare Au-based SPR chip, the GO-based SPR chip had ultrahigh sensitivity to detect biomolecules.

In addition to the development of highly sensitive measurement techniques, we also successfully developed carboxyl-GO for use in an immunoassay biosensor.[15] Most of the reported surface plasmon resonance (SPR)-based biosensors have used graphene,[16,17] reduced GO,[18,19] graphene-decorated metal nanoparticles,[13,20] or MoS_2-COOH as the sensing film chip.[21] Moreover, novel strategies for the synthesis of surface functionalized graphene oxide (fGO) sheets have used a modification/doping process to improve the electronic carrier properties via oxidizing (p-doping) or reducing (n-doping) enhanced charge trapping at the interfaces,[22] or regulating the energy gap shift to a visible light wavelength[23] or enhancing the excellent photocatalytic features for bio-sensing applications.[24,25] In addition, more effective modification of the fGO sheets can be achieved on vicinal surfaces, selected using colloid chemistry or chemical compound methods with functional molecules, and also synthesized via self-assembly of organic molecules to enhance the highly sensitive detection. The most promising aptamer peptide-based biosensors are currently aptasensors, due to advantages such as cheap production, high purity, resistance to high temperatures and easy synthesis. In addition, the high selectivity and specificity of peptide binding to a protein represents a significant challenge for molecular diagnosis applications, which can be achieved by immobilization on a sensor surface with the correct orientation.[26] Therefore, the application of molecular detection technology has been widely studied. Other peptide-based SPR biosensors have been used to detect heavy metals,[27,28] the real-time detection of breast cancer,[29] staphylococcal enterotoxin B,[30] and peptide-Au nanorods to detect cardiac biomarkers.[31] In addition, the peptide-graphene based combination has uniquely excellent properties for use in non-immunological biosensors,[32,33] antimicrobial,[34] and drug carriers.[35] These techniques are currently limited to standard recombinant protein tests, and they have not yet been tested in clinical sera for diagnostic studies. As a clinical molecular diagnostic tool, an SPR-peptide based biosensor appears to be a very promising diagnostic technology. However, few SPR-peptide biosensors have been developed as clinical blood diagnostic tools, especially to detect relevant disease biomarker proteins in the blood of pregnant women. Of these biomarkers, human chorionic gonadotropin (hCG) is a very important protein which can be used to detect pregnancy and related morbidities such as ectopic pregnancy,[36] miscarriage,[37] fetal abnormalities,[38] and testicular tumors.[39] Therefore, the development of a highly sensitive and rapid detection diagnostic chip to estimate the amount of hCG protein is necessary. The hCG protein is a hormone essential for the maintenance of pregnancy and the development of both placenta and fetus. Therefore, the development of an SPR biosensor for hCG determination in blood is a very significant task. Recently, a few peptide aptamer based biosensors have been found and used as the recognition elements for binding to hCG proteins. For example, Ding et al reported a LC-based immunoassay method to detect hCG, a limit of detection (LOD) is approximately 1 IU/mL (2 nM).[40] Chang et al reported a colorimetric detection of hCG-binding peptide aptamer and utilized this in catalytic gold nanoparticles (Au NPs)-based assay, a LOD of 15 mIU/mL (1.5 ng/mL) can be achieved.[41] Xia et al reported silver nanoparticles (Ag NPs)-based colorimetric assay method to detect hCG, a LOD of 0.4 mIU/mL was achieved.[42] In our previous study, we reported a graphene oxide (GO) SPR biosensor based on a peptide aptamer for hCG assay with a detection limit of 0.065 nM (3.25 ng/mL, 32.5 mIU/mL).[14] The detection limit of hCG serum test in quantitative ELISA is 0.5 ng/mL (5.0 mIU/mL). To date, no peptide-based or graphene-based SPR biosensor has been reported for the detection of hCG in clinical blood samples.

In this study, we developed an ultra-sensitive SPR aptasensor using a non-labeled and non-immunological method involving functionalized carboxyl-GO modification binding peptide techniques. This sensor was shown to be a sensitive and robust tool for the detection and quantification of low levels of hCG in clinical blood

serum samples. The carboxyl-GO composite was shown to have biocompatible surfaces beneficial for the detection of covalently-linked peptides in biosensor technology. The peptide was immobilized on the carboxyl-GO surface of the SPR biosensor and had a highly selective and specific interaction with the hCG protein. We used two types of detection methods with standard samples and clinical samples. There were two aims: First, to detect hCG protein in phosphate-buffered saline (PBS) buffer. Since the hCG in the test sample was diluted with PBS, it was relatively simple to detect. Therefore, there was no interference of other protein molecules in the detection. This experiment did not use bovine serum albumin (BSA) to reduce non-specific binding. Second, to detect hCG protein in clinical specimens. Because the doped clinical samples contained interfering proteins and other molecules that could have caused electrostatic interference and affect SPR detection, BSA was used in this experiment to reduce non-specific binding in the PBS solution. The selectivity of the SPR aptasensor was evaluated by comparing the sensor responses to BSA and human serum albumin (HSA).

Materials and methods

Preparation of the SPR aptasensor and hCG detection method in PBS buffer samples

Modification of the GO sheets was carried out using chloroacetic acid ($ClCH_2CO_2H$, Alfa Aesar, Ward Hill, MA, USA), which hydroxyl (–OH), epoxide (–O–), and ester groups into the carboxyl group (–COOH).[15,43] The main synthesis steps for the conversion of GO to carboxyl-GO are shown in Figure 1A and B. GO solution at a concentration of 2 mg/mL in a volume of 5 mL was prepared and shaken with ultrasound at 350 W for 1–2 hrs to break the GO sheets into flakes of less than 1 μm. This was followed by the addition of 1.0 g of $ClCH_2CO_2H$ and 1.2 g of sodium hydroxide (NaOH) to the GO aqueous suspension in an orbital shaker (swing type) with shaking for 4 hrs at 60 °C. A centrifuge was then used to repeatedly remove the $ClCH_2CO_2H$ and NaOH with deionized water. Finally, deionized water was added to achieve a carboxyl-GO solution concentration of 1 mg/mL. The carboxyl-GO-based SPR chip was chemically modified using a 47 nm Au electrode with thiol- and amine-group self-assembled monolayers (SAMs) of cystamine (Cys) (cystamine dihydrochloride 98%, Alfa Aesar, Ward Hill, MA, USA). The Au electrode was immersed in a double-distilled water (ddH_2O) Cys solution diluted to 10 mM for 24 hrs at room temperature. The Au/Cys chip was then immersed in aqueous carboxyl-GO (1 mg/mL) suspension for 5 hrs followed by thorough rinsing with deionized water to remove unbonded carboxyl-GO, resulting in Au/Cys/carboxyl-GO film. As shown in Figure 1C, the first step of enabling carboxyl-GO biological binding was the activation of the –COOH terminal group for direct conjugation to amine ($–NH_2$) bonds to allow for a better affinity

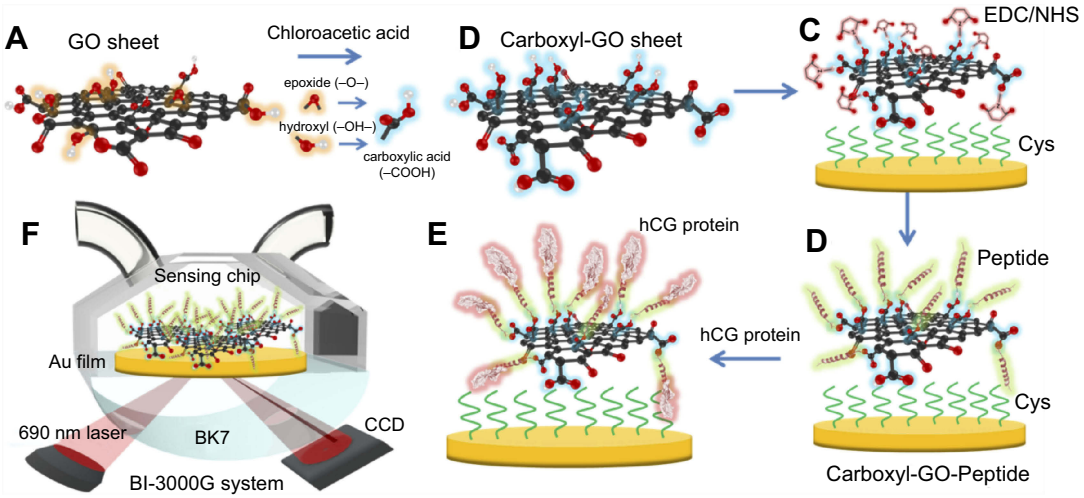

Figure 1 Schematic illustration of the conversion of (**A**) GO into (**B**) carboxyl-GO sheets via a facile one-step chloroacetic acid modification route at low temperature. (**C**) Carboxylic acid-terminated groups were formed and then activated with EDC/NHS to form an NHS ester-terminated group at the carboxyl-GO surface. (**D**) The attachment of peptides via amine coupling, and the deactivation of the unreacted surface sites with ethanolamine (EA) blocking. (**E**) Immobilization of the peptide on the carboxyl-GO-based SPR chip using non-immunological to detect hCG protein. (**F**) Schematic instrumental set-up of the Kretschmann configuration, the carboxyl-GO-peptide film was immobilized on the chip and injected into the hCG protein interaction of the SPR flow cell. The flow rate was 30 μL/minute, and the running buffer was phosphate-buffered saline (PBS) solution.
Abbreviations: GO, graphene oxide; hCG, human chorionic gonadotropin; SPR, surface plasmon resonance.

reaction. The carboxyl-GO sheets were activated with a 1:1 mixture of 0.1 M N-hydroxysuccinimide (NHS) and 0.4 M l-ethyl-3-(3-dimethyl aminopropyl) carbodiimide (EDC), followed by the injection of 200 μL of the EDC/NHS solution to activate the –COOH surface at room temperature at an injection flow rate of 30 μL/minute.

To develop a SPR aptasensor for short oligopeptide sequences,[40] we used (N-)PPLRINRHILTR(-C) to assay hCG protein. The structural feature of this unique short oligopeptide sequence allows peptide aptamers to bind with the hCG target protein with strong affinity and high specificity. A 100 μM injection of peptide at a flow rate of 30 μL/minute was first immobilized onto the carboxyl-GO surface in SPR flow channel-1. Furthermore, we used 200 μg/mL of BSA protein to block the Cys linker and did not immobilize the peptide probe in flow channel-2, as shown in Figure 1D. To deactivate the NHS ester-terminated groups on the surface that did not react with the peptide, 1 M ethanolamine (EA) solution dissolved in phosphate-buffered saline (PBS) solution was injected over the sensing film at a 30 μL/minute flow rate followed by blocking. This reduced the negative charge of the sensing film surface and thus decreased the potential for non-specific binding. Figure 1E shows the interaction of the protein with the peptide using injections of different concentrations to detect 200 μL hCG protein at a flow rate of 30 μL/minute. This was followed by further washing with a 1x working concentration of PBS running buffer at a flow rate of 30 μL/minute. Figure 1F shows that the carboxyl-GO-peptide based SPR sensing system was designed based on double flow channel detection using a 690 laser source, employed to angularly resolve SPR sensing in a BI-SPR 3000 dual-channel instrument (Biosensing Instrument Inc., Tempe, AZ, USA).

Preparation of the carboxyl-GO-based chip in clinical samples detected

In clinical samples experiments, different from the detection in PBS buffer samples, we add a step by using 200 μg/mL of BSA protein blocking to reduce non-specific binding (NSB). This is an important step when performing SPR clinical samples experiments.[44] In an assay with a serum sample, the addition of BSA and Tween-20 (NO. P9523, Sigma-Aldrich, St. Louis, MO, USA) to the blood serum samples was found to improve hydrophobic interactions with other proteins, and charge interactions of NSB of serum proteins with the sensing surface in each experiment. The running buffer (PBBT buffer) was composed of 1x PBS, 0.05% Tween-20, and 600 μL of BSA protein mix at a concentration of 1 mg/mL in a volume of 100 cc to prevent NSB in the human serum and to prevent the proteins from binding to the carboxyl-GO surface. In all experiments, the injection volume was 200 μL and the flow rate was set at 30 μL/min and regeneration solution was 50 mM of NaOH at pH 12.0. The blood serum samples from normal pregnant women at an average gestational age of about 14 weeks were used in this study. The concentration of hCG protein in these serum samples was obtained using ELISA. hCG is a glycoprotein hormone consisting of two non-covalently bound subunits, with a molecular weight of approximately 36 kDa. All of the blood serum supernatant samples were diluted using PBBT buffer to a achieve a series of samples with different concentrations of hCG to minimize the adverse effects of high viscosity on carboxyl-GO sensing performance. Therefore, the detection of blood serum hCG was carried out in the PBBT running buffer, which was designed in such a way as to remove nonspecifically adsorbed proteins while not disrupting the binding of hCG to peptides immobilized on the sensor surface.

Results

Analysis of chemical bonds and morphology of carboxyl-GO sensing films

The self-assembly of carboxyl-functional groups in aqueous suspension with the assistance of chloroacetic acid was demonstrated to be a powerful method to build the carboxyl-GO architecture. The exact carboxyl transformation procedures were verified with different characterization methods. Figure 2A shows the attenuated total reflectance Fourier transform infrared spectroscopy (ATR-FTIR) spectra of the carboxyl-GO, GO and rGO films at three different chip processing conditions. The properties of the primary carboxyl-GO functional groups including epoxide groups (–O), hydroxyl groups (–OH) and carboxylic acid groups (–COOH) on the surface showed the following characteristic features: C–O–C vibrations in the epoxide groups, including the vibration modes of epoxide ring-opening bonds (at 910 cm^{-1}); hydroxyl groups originating from alkoxy bond C–O vibrations of C–OH (C–OH at 1,064 cm^{-1}); tertiary alcohol bonds (CH_3–OH at 1,380 cm^{-1}); an O–H vibration of the C–OH groups (at 1,455 cm^{-1}); alkyl C-H stretch (CH_2 at 2,850~2,920 cm^{-1}); and phenol bonds (Ar–OH

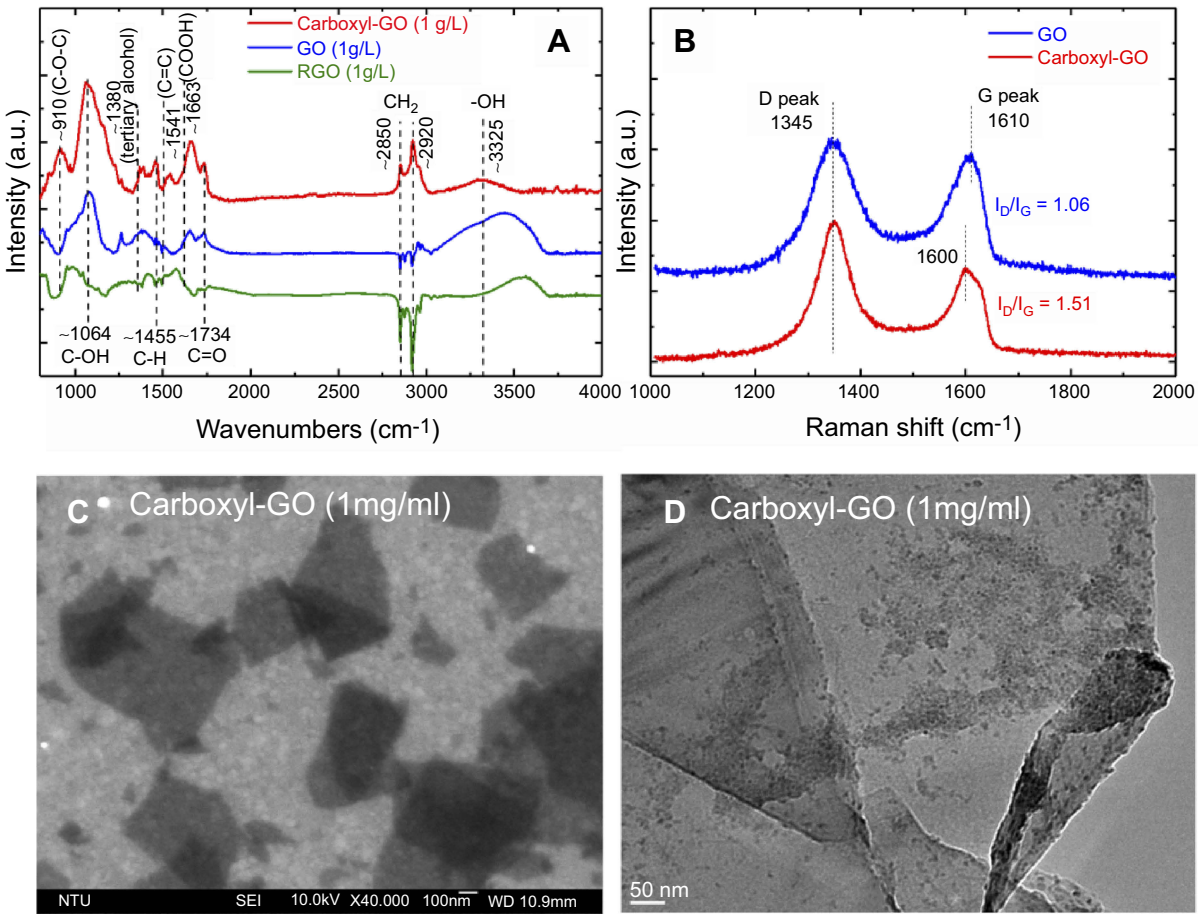

Figure 2 A scheme for the preparation of either functional carboxyl-GO modified (**A**) FTIR spectra, (**B**) Raman spectra, (**C**) SEM, and (**D**) TEM images.
Abbreviations: FTIR, Fourier transform infrared spectroscopy; SEM, scanning electron micrograph; STM, transmission electron microscopy.

at 3,050–3,800 cm^{-1}). A carboxyl stretching vibration of O–H bending of the C–OH group (–COOH at 1,663 cm^{-1}) was detected at the edge, along with ketone species (C=O) (1,734 cm^{-1}), and sp2-hybrided C=C (1,541 cm^{-1}, in-plane vibrations).[45] Therefore, Figure 2A reveals significant increases in the C–OH (C–OH at 1,064 cm^{-1}), C–OH group (–COOH at 1,663 cm^{-1}) contents (reductions in the Ar–OH at 3,050–3,800 cm^{-1}), confirming the carboxyl-functionalization of GO sheets is successful.

Figure 2B shows Raman results of GO and carboxyl-GO. The Raman peaks of GO, showed the D (the arises from breathing mode of κ-point photons of A1g symmetry) peak as the characteristic feature at 1,345 cm^{-1} and the prominent G (the E2g mode of sp2 carbon atoms) peak as the characteristic feature at 1,610 cm^{-1}. The intensity of the prominent D peak (1,345 cm^{-1}) was comparable with that of the G peak (1,600 cm^{-1}) and their large bandwidths revealed structural defects in carboxyl-GO. This change in the ratio (I_D/I_G) of intensities of the D and G bands is attributed to the increase in defect concentration from GO to carboxyl-GO. The relative I_D/I_G ratio is a measure of the defects present on graphene structure, which means that the sp2 bond is broken, and in turn means more sp3 bonds. The number of sp3/sp2 bonds was obtained from the Raman spectral peak intensity ratio (I_D/I_G). Extensive oxidation reduced size of the in-plane sp2 domains. The increased I_D/I_G ratio in Raman spectra sp2 and sp3 suggests a decrease in the average size of the sp2 domains upon reduction of the exfoliated GO, perhaps indicating that new, more numerous but smaller graphitic domains were created.[11,46] The ratio I_D/I_G equals the sp3/sp2 bond ratio in the carboxyl-GO. The I_D/I_G ratio for GO is 1.06, and for carboxyl-GO is 1.51. That of carboxyl-GO has a higher I_D/I_G owing to the presence of unrepaired defects following the chemical modification involves the –OH, –O–, and ester groups into the carboxyl groups. Figure 2C shows representative scanning electron micrograph (SEM) image of the carboxyl-GO sheets, revealing a granular morphology with small clusters of irregular particles, some of which were in the nanoscale.

The carboxyl-functional groups presenting as irregular particles were similar to the organic matrix-mediated biomineralization of mollusk shells on a transmission electron micrograph (TEM) image as shown in Figure 2D.[47]

X-ray photoelectron spectroscopy analysis of carboxyl-GO sensing films

The carboxyl-GO biocompatible composites were synthesized using the modified Hummer method and then alkylated using chloroacetic acid under basic conditions. Figure 3 shows the presence of carbon and oxygen elemental and chemical state analyses in the carboxyl-GO film using X-ray photoelectron spectroscopy (XPS). Figure 3A shows the XPS spectrum of carboxyl-GO including various nitrogen and oxygen peaks and a carbon peak in the three different sensor chips for Au/Cys/carboxyl-GO/peptide, Au/Cys/carboxyl-GO, and Au/Cys/peptide, respectively. Figure 3A shows the survey, carbon of C 1s (285 ev), nitrogen of N 1s (400 ev), and oxygen of O 1s (532 ev) peaks in the XPS spectra of the chips, respectively. Along with the C, N and O peaks, the spectra contained sulfur S 2s (238 ev), which was caused by the -SH of the Cys linker. In addition, the contents of O 1s in the Au/Cys/carboxyl-GO/peptide and Au/Cys/carboxyl-GO chips were particularly high, which was caused by the oxide of carboxyl-GO.

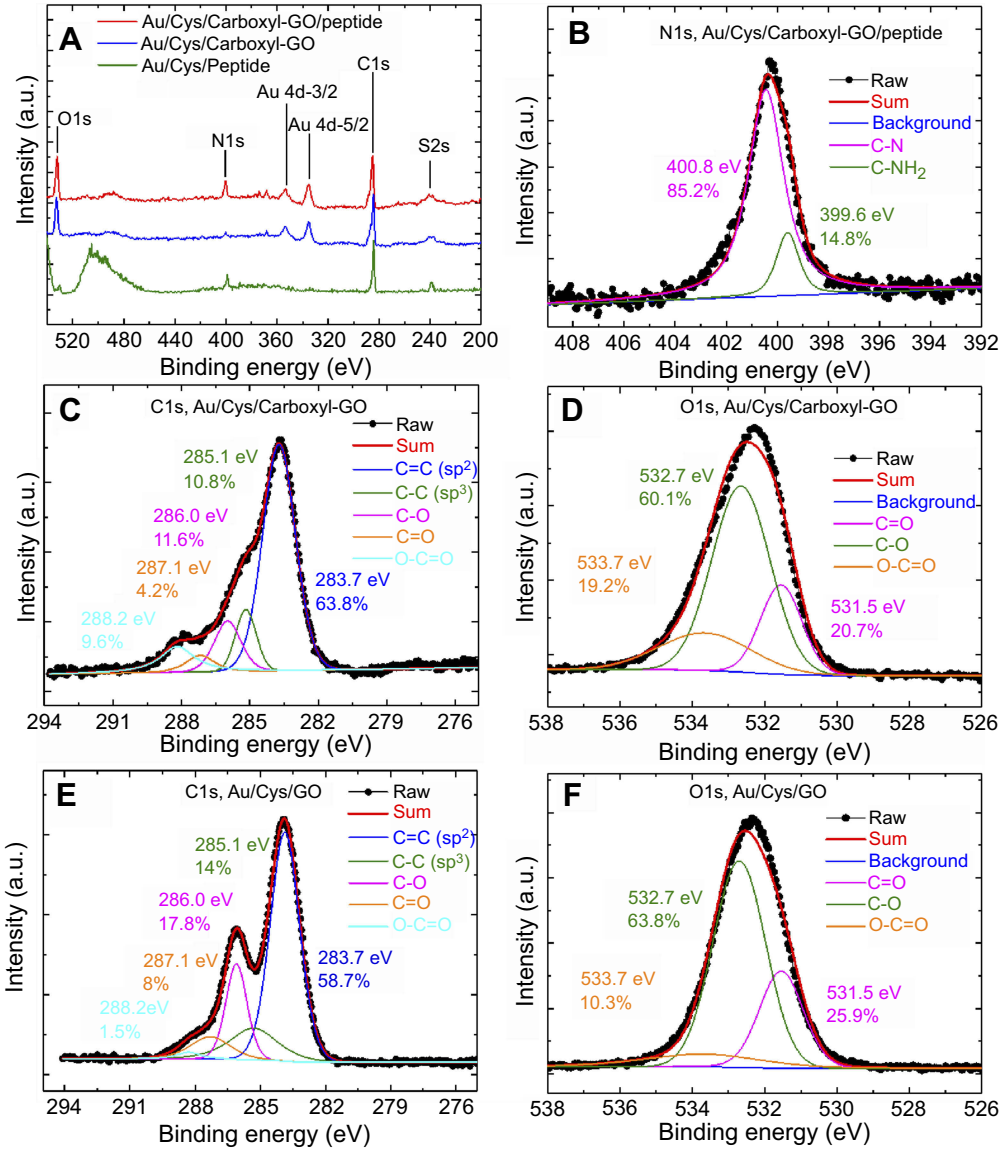

Figure 3 High resolution XPS spectra of the carboxyl-GO and GO films. (**A**) Survey scan XPS spectra of the different sensing chips. (**B**) N1s region for the as-formed carboxyl-GO/peptide chip. (**C**) C1s and (**D**) O1s regions for the as-formed carboxyl-GO chip. (**E**) C1s and (**F**) O1s regions for the as-formed GO film.
Abbreviations: XPS, X-ray photoelectron spectroscopy; GO, graphene oxide.

The nitrogen (N1s) component was caused by immobilization of the peptide molecule on the carboxyl-GO surface. As shown in Figure 3B, the N 1s region of the XPS patterns of the carboxyl-GO/peptide chip could be fit using deconvolution into two peaks attributed to two different nitrogen-containing groups: C–N (400.8 eV, 85.2%) and C–NH_2 (399.6 eV, 14.8%). However, it was possible to identify amide and amine binding energies at 399.6 eV and 400.8 eV, respectively. This is consistent with previous studies.[48,49]

The XPS spectrum and deconvoluted C1s and O1s spectra are shown in Figure 3C and D. The XPS spectra of C 1s for carboxyl-GO were deconvoluted into five peaks, 283.7, 285.1, 286.0, 287.1 and 288.2 eV, corresponding to the characteristic peaks of C=C (63.8%), C-C (10.8%), C-O (11.6%), C=O (4.2%), O-C=O (9.6%), respectively, and the relative peak area of carbon atoms bonded to carbon in the carboxyl-GO structure. The XPS spectrum for C1s (Figure 3C and E) shows the different chemical environments of the carbon atoms bonded to carbon in carboxyl-GO and GO structures. The peak (288.2 eV) in the spectrum of O-C=O contents corresponded to 9.6% and 1.5% carboxyl-GO and GO, respectively. This showed that COOH was successfully modified on the GO surface. Figure 3D and F show the O1s XPS spectra for carboxyl-GO and GO, which revealed a significant degree of oxidation as indicated by the numerous oxygen-containing groups; peaks at 531.5, 532.7 and 533.7 eV were assigned to oxygen atoms in C=O, C-O and O-C=O, respectively. Figure 3D results showed that carboxyl-GO contained significant amounts of O-C=O and C-O (19.2% and 60.1%, respectively), signifying that most of the carboxyl modified on the GO surface was arranged in the structure.

Electrochemical and SPR analysis of carboxyl-GO sensing films

To evaluate the electrochemical performance of the as-prepared sensing chips, cyclic voltammetry (CV) curves were measured. Figure 4(A–C) show the results of the cyclic voltammograms (CV) of the different sensing layers obtained at a potential ranging from 0.0 to 0.7 V and scan rate of 10, 25 and 50 mV/s in 0.1 M KCl solution that also contained 2 mM $[Fe(CN)6]^{3-/4-}$, with the frequency ranging from 100 mHz to 100 kHz at 5 mV. Quantitative real-time EC-SPR detection was performed in a 2 mL internal sample volume cell using an integrated system including a CHI-604D electrochemical analyzer work station (CH Instruments Inc., Austin, TX, USA) and BI-3000G SPR Instrument (Biosensing Instrument Inc., USA). In the electrochemical experiment, a three-electrode system was used including the modified Au/carboxyl-GO electrode as the working electrode, platinum (Pt) wire as the counter electrode, and Ag/AgCl (saturated KCl) as the reference electrode.

The CV curve revealed a quasi-rectangular shape, indicating that the carboxyl-functional groups had maintained good charge propagation within the film. Among them, the difference between the two peak potentials $\Delta E_p=|E_{pc} - E_{pa}| =59/n$ mV was of particular interest (where ΔE_p is potential separation, E_{pa} is anodic peak potential, and E_{pc} is cathodic peak potential, the case of n electrons).[50,51] This difference in peak potentials ΔE_p mainly resulted from the effects of sensing film revealing the electrochemical reversibility. Figure 4A shows that ΔE_P-values at a scan rate of 10 mV/s were 0.08, 0.063, 0.086, and 0.096 for the bare Au, Au/Cys, Au/Cys/carboxyl-GO, and Au/Cys/arboxyl-GO/peptide sensing chips, respectively. Figure 4B shows that ΔE_P-values at a scan rate of 50 mV/s were 0.103, 0.09, 0.086, and 0.122 for the bare Au, Au/Cys, Au/Cys/carboxyl-GO, and Au/Cys/carboxyl-GO/peptide sensing chips, respectively. This result shows that the electron transport rate of the Au/Cys/carboxyl-GO/peptide sensing chip was hindered due to the adsorption of 100 μM of peptides. This result shows that the peptides cause a decrease in current and an increase in the potential difference of ΔE_p. Figure 4C shows that the CV curves of the Au/Cys/carboxyl-GO/peptide chip at a 50 mV/s scan rate were also affected by the intrinsic barrier for electron transfer. The corresponding ΔE_p-values were 0.096, 0.096, and 0.122 V for 10, 25, and 50 mV/s scan rates, respectively.

Figure 4D shows the results of the electrochemical impedance spectroscopy (EIS) analysis recorded for all of the sensing chips at frequencies from 1 Hz to 100 KHz, an initial potential of 0.24 v and 12 points per decade under excitation of the amplitude when the input ac signal was kept at 5 mV in the presence of equimolar 2 mM $[Fe(CN)6]^{3-/4-}$. By fitting the semicircular diameters corresponding to the interfacial electron-transfer resistance at Rct for the bare Au, Au/Cys, Au/Cys/GO, Au/Cys/carboxyl-GO, and Au/Cys/carboxyl-GO/peptide chips, the values were 27.46, 67.97, 1015, 226.57, and 326.45 Ω, respectively.

The experimental results showed that the added modified Cys and GO, or GO-COOH layer by layer on the bare

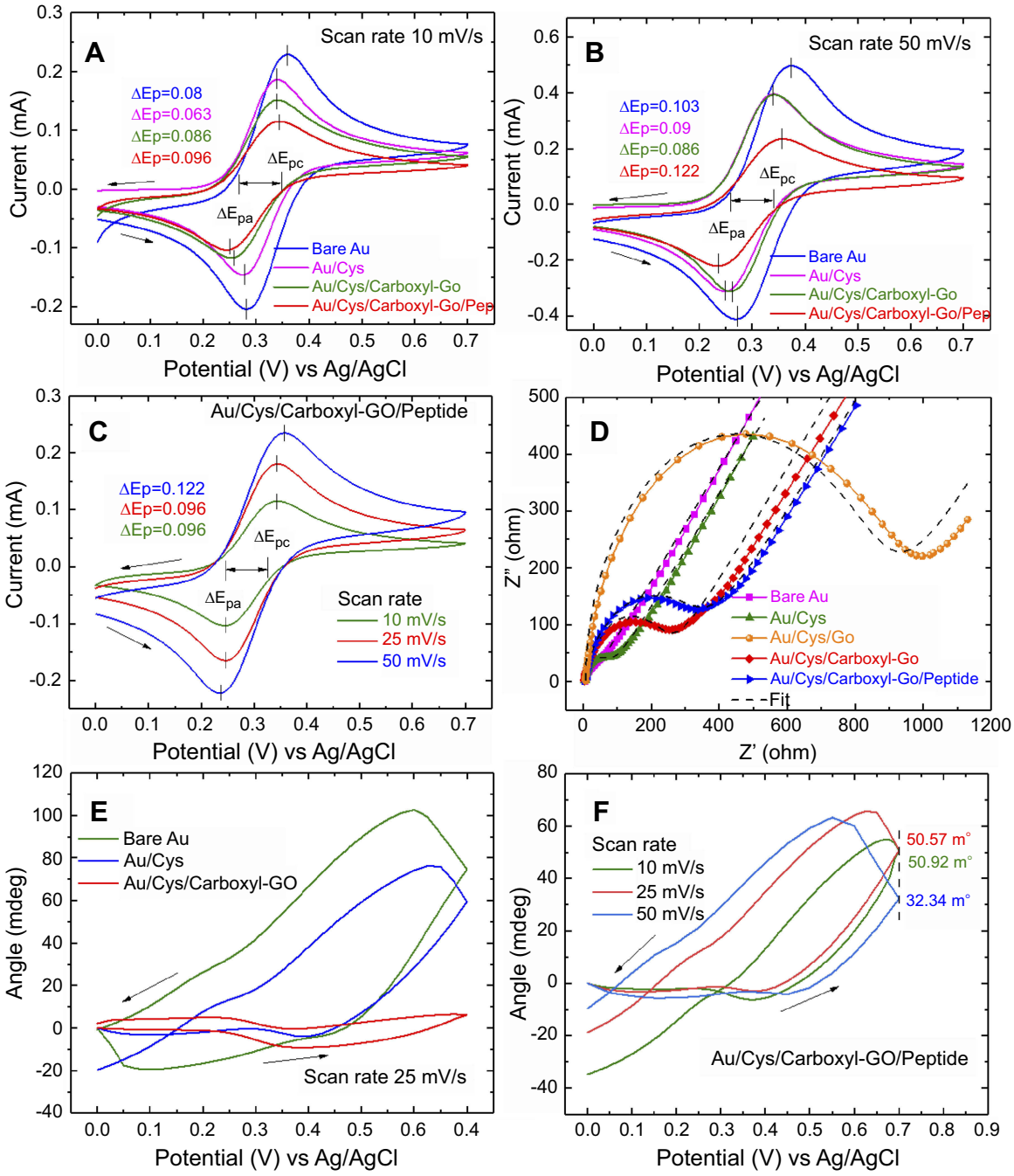

Figure 4 Cyclic voltammograms of bare Au, Au/Cys, Au/Cys/carboxyl-GO, and Au/Cys/carboxyl-GO/peptide chips at scan rates of (**A**) 10 mV/s and (**B**) 50 mV/s. (**C**) Cyclic voltammograms of the Au/Cys/carboxyl-GO/peptide chip with increases in scan rate from 10 to 50 mV/s. (**D**) The EIS spectra of the different sensing chips. (**E**) CV-SPR voltammograms of the different sensing chips at a potential scanning rate of 25 mV/s. (**F**) CV-SPR voltammograms of the Au/Cys/carboxyl-GO/peptide chip at different scan rates.
Abbreviations: Au, gold; Cys, cystamine; GO, graphene oxide; EIS, electrochemical impedance spectroscopy; CV, cyclic voltammetry; SPR, surface plasmon resonance.

Au electrode, which resulted in the impedance appeared to be larger because the oxide could hinder electron transfer. Compared with Au/Cys/GO electrodes, the results showed that the Rct values of carboxyl-GO film had effectively decreased, and that the –COOH improved the electroactive surface area which contributed to the more conductive pathways for electron transfer. These findings show that carboxyl-GO could be used as a modifier to construct biosensors with improved performance.[13,14,52]

Surface modification of GO by negatively charged carboxyl-groups to yield carboxyl-GO could further improve aqueous dispersion, increase conductivity and enhance biological affinity, providing reactant sites for conjugation with positively charged peptides, plus further

functionalization sites for covalent bioconjugations to the activated carboxyl group.[52] In addition, improving the optical conductivity and electrical conductivity of graphene effectively enhanced the sensitivity of sensing.[53] These results provide proof that the conductivity of the surface improved performance of the SPR biosensor.[53,54]

Figure 4E and F show the CV scan voltage-based SPR voltammograms of the different sensing chip redox reactions at different potential scan rates. We used carboxyl-GO due to its remarkable environmental chemical stability, and the drastic change in its electrical conductivity upon simple oxidation and reduction. Moreover, redox reactions in peptide molecules are known to cause conformational changes, although these changes are often very small. However, they can be studied using real-time EC-SPR at different scan rates to measure potential and angle shift. Real-time EC-SPR uses the combination of CV and SPR to monitor interactions of carboxyl-GO and peptide aptamers on the surface of bare gold. Specifically, electrochemistry is the analysis of the rate of permeation reaction of electrons on carboxyl-GO and peptide aptamers, while SPR simultaneously monitors the reaction characteristics of the electric double layer of ions of the peptide aptamers in real time. Therefore, In CV-SPR voltammograms of modified sensing film measurements, the potential-induced SPR angle shift ($\Delta\theta_{SPR}$) of the sensing surface-electrolyte interface could be controlled, which induced various interesting phenomena. For example, simple double potential (ΔV_d) could induced SPR angle shift ($\Delta\theta_{SPR}$) via sensing film changes in the refractive index (Δn), changes in the average adsorbed monolayer thickness (Δd_s), and surface charge density (Δn_e) of the sensing film. Among these factors, the relationship between Δn_e and the interface property of $\Delta d_s = -C_d (\Delta V_d/e\ \Delta n_e)$, where C_d is the double layer capacitance, the CV-SPR signal was proportional to the potential-induced SPR angle shift given by[55,56]

$$\frac{\Delta\theta_{SPR}(\lambda)}{\Delta V} = c_1\frac{\Delta n(\lambda)}{\Delta V} + c_2\frac{\Delta d_s}{\Delta V} + c_3\frac{\Delta n_e}{\Delta V} \qquad (1)$$

where c_1, c_2, and c_3 are constants and λ is the wavelength of the incident light. The potential-induced SPR angle shift was mainly caused by differences in the refractive index between the reduced and oxidized forms of the sensing film complex, but it was also affected by the double layer charging effect.

The CV-SPR voltammograms are presented in Figure 4E, which shows significant influence on the trend of potential-induced SPR angle shifts as the double layer proportionality constant between $\Delta\theta_{SPR}$ and ΔV_d is known to be determined by the values of C_d and Δd_s. Figure 4E clearly shows that in the bare Au chip at a scan rate of 25 mV/s, C_d and d_s were greater than and in the other two sensing chips, thus leading to a large angle shift of SPR. We also analyzed the SPR signals of Au/Cys and Au/Cys/carboxyl-GO chips, and found two phenomena of note. First, the SPR angle shift attributed to the double layer existing large charging effect in the oxidation reaction (from 0.0 to +0.7 V) became even smaller, which was expected due to the decrease in interfacial capacitance. Second, the SPR angle shift associated with the reduction reaction (from +0.7 to 0.0 V) also decreased significantly due to blockade of the reduction reaction by the Cys/carboxyl-GO film. This result is consistent with the EIS in Figure 4D.

Figure 4F shows the CV-SPR voltammograms of the Au/Cys/carboxyl-GO/peptide chip at three different scan rates of 10, 25, and 50 mV/s, which showed potential-induced SPR angle shift at 50 mV/s. When the scan potential was the oxidation reaction, the SPR angle changes were 50.92, 50.57, 32.34 mdeg for the 10, 25, and 50 mV/s scan rates, respectively. When the scan potential was the reduction reaction, the SPR shifts were observed at −34.82, −18.77, and −9.6 mdeg for the 10, 25, and 50 mV/s scan rates, respectively, which was mainly due to the double charging effect described by Equation (1). The potential-induced SPR angle shift was mainly affected by d_s and C_d of the sensing film.

Analysis of the interaction between carboxyl-GO sensing film and peptide

Comparisons of the SPR angle shift were performed using the peptide aptamer in three different chips as shown in Figure 5A. The SPR sensorgram showed that the injected peptides at a flow rate of 30 μL/min resulted in SPR angle shifts on the three different sensing chips of 20.51, 14.03, and 9.64 mdeg for the Au/Cys/carboxyl-GO, Au/Cys/GO and convention chips, respectively. These results showed that the carboxyl-GO-based SPR chip had a high affinity binding reaction.

We individually injected the peptides at different flow rates to observe the binding reaction with carboxyl-GO affinity interaction kinetic analysis. Figure 5B shows that with injection at a flow rate of 30 μL/minute the SPR equilibrium contact angle (θ_{eq}) exhibited a large shift of 22.37 mdeg at 300 s. In addition, at flow rates of 60 and 90 μL/minute at 200 s the θeq values were 10.68 and 10.01

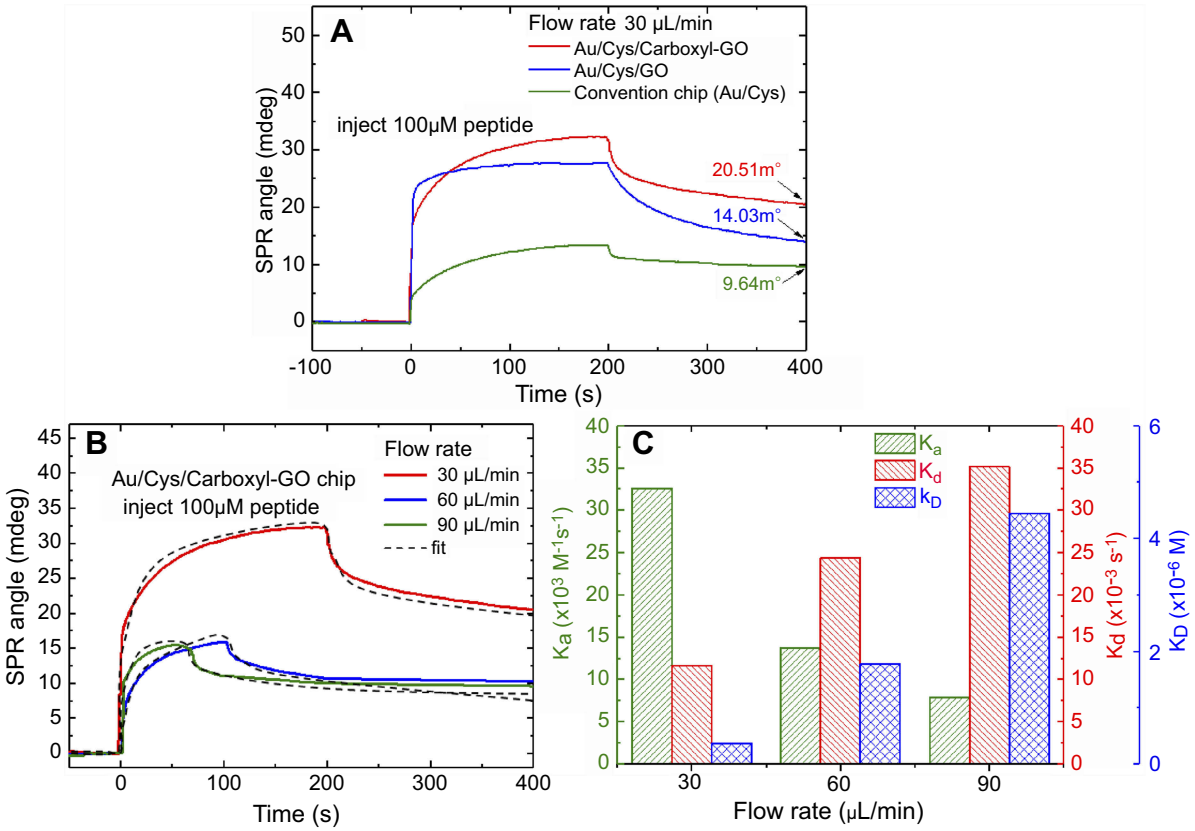

Figure 5 (**A**) The injection of peptides at a flow rate of 30 μL/min showing the three different SPR chip binding reactions. (**B**) The injection of peptides at different flow rates showing the carboxyl-GO ship binding reaction. (**C**) The binding kinetic constants at different flow rates in association and dissociation analyses.
Abbreviation: GO, graphene oxide.

mdeg, respectively. The peptide aptamer had strong adhesion at a flow rate of 30 μL/min, at which a maximum response in SPR angle shift was reached. Flow rates of 60 and 90 μL/min resulted in a gradual decrease in the SPR response. The results showed that the carboxyl-GO with peptide aptamer interface reaction rate was not suitable for more than 30 μL/min. The experimental results are consistent with previous studies.[57,58]

From the different flow rates we calculated the binding kinetics. We performed a 1:1 interaction of the SPR biosensor in carboxyl-GO with peptide molecule using the binding Langmuir model.[59] The binding kinetics parameters of the association rate k_a, dissociation rate k_d, and dissociation constant K_D (k_d/k_a) for the interaction of carboxyl-GO with peptide aptamer are shown in Figure 5C. At a flow rate of 30 μL/min, the value of K_A was 2.81×10^7 M^{-1} and that of K_D was 0.36×10^{-7} M, which was in good agreement with the calculated fit. The results showed that these values were comparable to the highest seen for natural biological immunoassay systems.[58] By fitting the binding obtained under analogous conditions, the values of k_a were determined to be 32.57, 13.75 and 7.89×10^4 M^{-1} s^{-1} for flow rates of 30, 60, and 90 μL/min, respectively. In kinetic analysis of the peptide aptamer bonded on the carboxyl-GO based chip, an injection flow rate of 30 μL/min resulted in a large angle shift, and also a small K_D of 0.36×10^{-7} M compared to the other flow rates. This may be because the COOH-modified sensor chip caused interaction effects due to high affinity bonding.

Analysis of the carboxyl-GO/peptide assay of hCG protein in PBS buffer

We performed high affinity quantitative analysis for the binding, elution and regeneration kinetics of peptides and hCG protein assay as shown in Figure 6. The injecting 100 μM of the peptide at a flow rate of 30 μL/minute was immobilized onto the carboxyl-GO surface in both SPR flow channels. All assay experiments were conducted at room temperature using different hCG protein concentrations injected at a volume of 200 μL and a flow rate of 30 μL/minute. Figure 6A shows the SPR sensorgrams for hCG protein at assay concentrations of 2, 10, 20, 40, 80 and 100 pM on peptides immobilized with the carboxyl-GO

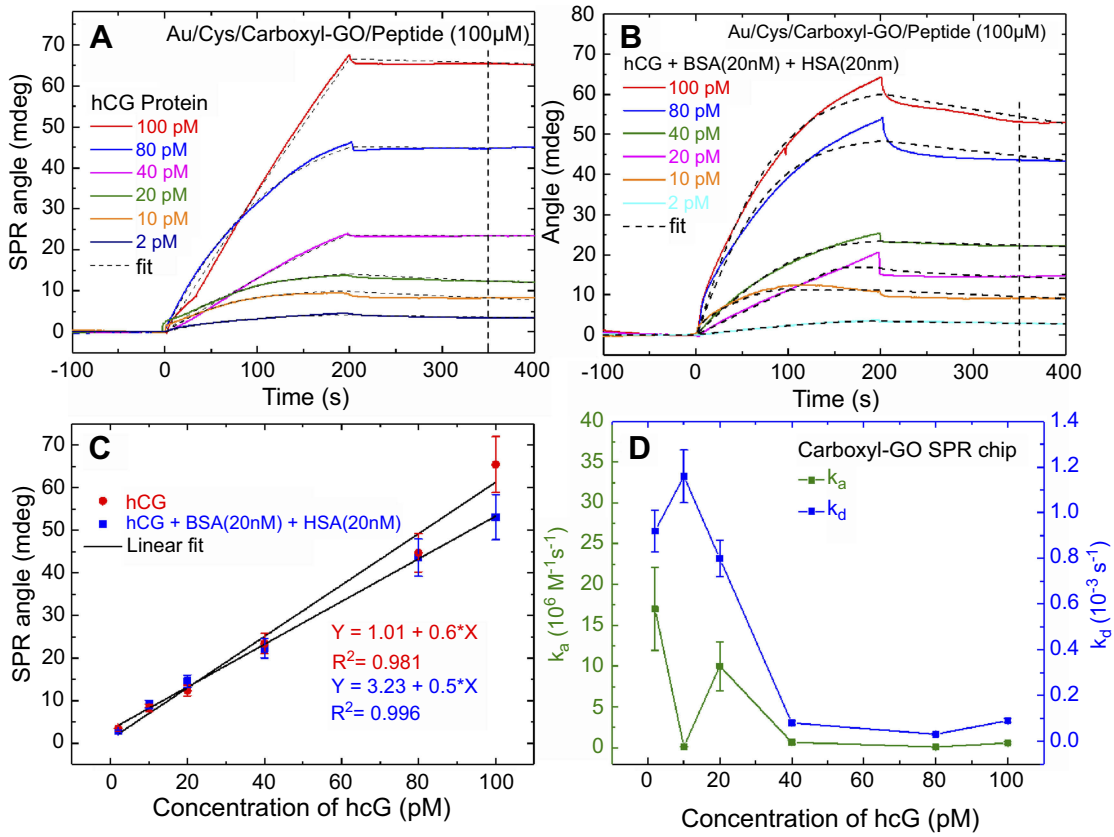

Figure 6 SPR sensorgrams for binding between peptides and hCG protein. The resonance angle shifts depended on (**A**) the carboxyl-GO chip with standard solutions of hCG concentrations alone, and (**B**) hCG mixed with BSA and HAS (20 nM each), respectively. (**C**) Characterization of peptide selectivity using both the single hCG protein and mixed protein experiments. (**D**) k_a and k_d values were obtained at different hCG protein concentrations by both kinetic and steady state fits.
Abbreviations: SPR, surface plasmon resonance; hCG, human chorionic gonadotropin; GO, graphene oxide; k_a, association rate constant; k_d, dissociation rate constant.

chip. Figure 6B and C show the SPR sensorgrams of the carboxyl-GO modified sensor chip for responses using 100 μM peptide to detect hCG protein concentrations in a mixture containing interfering proteins of 20 nM BSA and 20 nM HSA. Figure 6C shows the measured SPR angle responses in the linear fitting calibration curve. The carboxyl-GO chip showed a linear plot for hCG concentrations according to the linear regression equation y=1.01+0.6x and a correlation coefficient (R^2) of 0.981. The linear regression of the calibration curves was y=3.23+0.5x (R^2=0.996) for the adding interfering proteins BSA and HSA, where y represents the resonance angle shift, and x is the hCG concentration. There was clearly no significant interaction between the two proteins and the peptide in the mixed protein experiments, demonstrating the excellent selectivity and binding between the hCG protein and the peptide. The carboxyl-GO-peptide-based SPR biosensor with high-performance affinity was developed to characterize the binding and regeneration kinetics of immobilized carboxyl-GO-peptide and affinity assay. The result was more than the previous paper at flow rate of 60 μL/minute to immobilize the peptide (100 μM) at GO films to detect hCG protein as shown a LOD of 8.32 nM.[14] The stability of the resonance angle of the Au/Cys/carboxyl-GO/peptide chip in the buffer to detect the repeated regeneration of hCG protein was within 10%. Figure 6D shows that the binding kinetic constants of association rate constant (k_a) and dissociation rate constant (k_d) of 2 pM hCG on the carboxyl-GO-based SPR chip were 17×10^6 $M^{-1}S^{-1}$ and $0.92\times10^{-3}S^{-1}$, respectively. The error bars represent a range of 30% in the data, and at other concentrations were comparable in size to the data symbols. These results showed that the optimal carboxyl-GO chip had high resolution, binding affinity and slope of intensity mode.

Assay of hCG protein in clinical serum samples

The SPR sensorgrams showing the carboxyl-GO-based chip with interactions between specific peptides and clinical samples of hCG protein are shown in Figure 7. All clinical serum samples were measured using a 200 μL

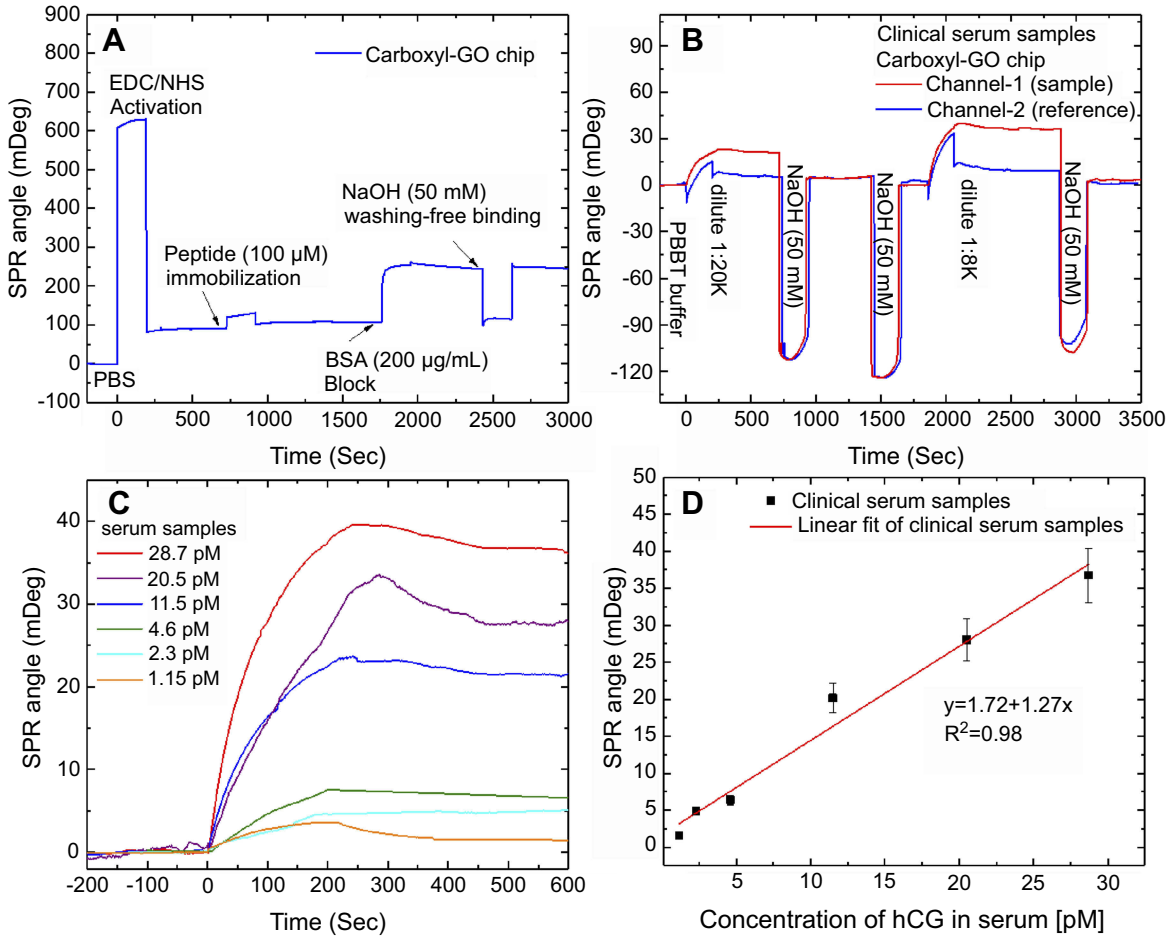

Figure 7 SPR sensorgrams of response curves for the assay of human hCG protein in the clinical serum samples. (**A**) SPR sensorgram of the peptide probe and BSA on the carboxyl-GO-based SPR aptasensor immobilization process steps of continuous reaction. (**B**) Sensorgram of two analysis cycles of a peptide–hCG protein interaction at different clinical serum sample concentrations. (**C**) The relationship between hCG protein and SPR angle shift was evaluated in serum samples with different dilutions. (**D**) Calibration plot for SPR angle shift with different dilutions of hCG serum samples at optimized conditions.

Abbreviations: SPR, surface plasmon resonance; hCG, human chorionic gonadotropin; GO, graphene oxide.

sample volume and a flow rate of 30 μL/minute. Figure 7A shows the SPR sensorgrams of using EDC/NHS to activate the surface and immobilize the peptide probe on the surface. Activation of –COOH and covalent coupling of the peptide probe and the use of BSA blocking to saturate free binding sites on the sensor surfaces or other protein binding surfaces reduced the handling of nonspecific bonds. Deactivation and the use of NaOH to wash away loosely associated peptide and BSA were performed for non-specific bonding treatment. The final response showed the immobilization of the sensing probe on the carboxyl-GO sensor chip in the channel-1 sensing area. In addition, there was no chemical modification in flow channel-2 and no immobilized peptide probe. Figure 7B shows the SPR sensorgram of using a continuous injection of the serum sample to assay human hCG protein. The SPR detection system was set up with a series of flow channels, and the injected sample flow direction was from channel-1 to channel-2. The PBBT running buffer was prepared by mixing PBS, BSA, and Tween-20.[44] The serum samples of the pregnant women at 14 weeks of gestation were diluted with different concentrations of 1:20 K and 1:8 K. The clinical serum samples were diluted in the PBBT running buffer. After injecting different concentrations of the serum samples of hCG, there were changes in the sensor response resulting in specific binding interactions of the peptide to the hCG protein. Washing of the non-covalently bound protein with 200 μL of 50 mM NaOH to regenerate the surface removed the serum sample completely and obtained the baseline value. The obtained results showed that channel-2 did not have any significant protein adsorption, and that interference of non-specific proteins did not significantly cause a reaction.

The concentration of hCG in the clinical serum samples was 230 nM (8.7 μg/mL) using ELISA. The clinical serum samples diluted to 1:8 K was equivalent to a concentration of 28.7 pM. After clinical serum samples were injected at a flow rate of 30 μL/minute, the sensor response gradually decreased due to spontaneous dissociation and became almost saturated within 500 s. The response curves of hCG protein flow at different dilutions (concentrations of 1.15–28.7 pM) are shown in Figure 7C. The carboxyl-GO films to detect hCG protein at a low flow rate of 30 μL/min as shows a LOD of 1.15 pM (0.575 mIU/mL). The results were more than the previous paper in a refrigerator at 4°C for 5 hrs to immobilize the peptide (1 mM) at GO films to detect hCG protein at a high flow rate of 60 μL/min as shown a LOD of 0.065 nM.[14] However, the response curve for a dilution of 1:200 K serum sample flow was clearly different from other dilutions, indicating that dissociation was promoted by hCG protein at a concentration with a limit of detection of 1:200 K (1.15 pM).

The result plotted as response (angle shift versus dilution of hCG serum sample, from the data recorded in Figure 7C) of the carboxyl-GO SPR aptasensor for the detection of hCG in the serum sample is depicted in Figure 7D. The SPR signal changed linearly with the linearity of the hCG protein concentration. The linear regression equations of the calibration curve were used to fit these data. The solid lines represent linear fits given by the equations, and were determined using data from all three experiments. When the dilution concentration of the clinical serum samples was between 1:8 K to 1:200 K, the linear regression equation was y =1.72 +1.27x, and the correlation coefficient was 0.98.

Comparing Figure 6C versus Figure 7D (calibration with standard solutions in buffer versus calibration in serum samples), Figure 6C clearly shows that the SPR angle shift decreased significantly (from 0.6 to 0.5 m/pM). The presence of hCG and other interfering chemical components in the serum sample solution caused the sensitivity in the serum samples to be slightly larger than in the buffered standard solutions (1.27 versus 0.6 m/pM) (Figure 7D). This was due to the effect of other chemical components in the serum such as proteins, fats, hormones, esters, enzymes, and inorganic substances causing a significant increase in non-specific responses. In addition, improving non-ionic Tween-20 concentrations, increasing ionic sodium dodecyl sulfate (SDS) and increasing the high flow rate could more effectively reduce and damage non-specific interference.

Conclusion

In this study, we demonstrated the potential of a carboxyl-GO-based peptide probe for use in a non-immune SPR aptasensor. The hCG is a well-established clinical biomarker of pregnancy and certain diseases. This sensor was an effective tool to investigate the mechanism of enhancing the assay efficacy of interactions between peptides and hCG protein with regards to affinity binding for a k_a of 17×10^6 $M^{-1}S^{-1}$. These results suggest that adding interfering proteins BSA and HSA did not have a significant effect on the interactions between hCG and peptides. The carboxyl-GO-based chip exhibited high charge-transfer properties, indicating that carboxyl-GO can improve electron flux and accelerate electron shuttle between the Au electrode substrate and the electrolyte. In standard solutions with different concentrations of hCG, the carboxyl-GO-based SPR aptasensor presented a response to hCG in the concentration range of 2–100 pM, with a correlation coefficient of 0.981. In clinical serum samples of hCG protein, the detection limit was below 1.15 pM (0.575 mIU/mL), well below the normal physiological level of hCG serum test in ELISA (0.5 ng/mL). The experimental results showed that the increased peptide immobilization can enhance the detection sensitivity. In the future, we believe that carboxyl-GO-based SPR aptasensors can be useful for the early clinical diagnosis of gynecological diseases and cancers, and that the potential clinical applications will benefit an ever increasing number of people and reduce the fatal threat of disease.

Acknowledgments

The authors would like to thank the Ministry of Science and Technology of the Republic of China, Taiwan, for financially supporting this research under Contract No. MOST 105-2221-E-003-027, and also Mackay Hospital (Project No. MMH-CT-10505). This work was approved by the Institutional Review Board (IRB) of Mackay Hospital for Human Clinical Trials (Permit Number: 15MMHIS020 and 15MMHIS115). We thank National Synchrotron Radiation Research Center (NSRRC, Taiwan) for the help in analyzing XPS spectra (National Synchrotron Radiation Research Center, Beamline 09A2 and 24A1).

Disclosure

The authors report no conflicts of interest in this work.

References

1. Dikin DA, Stankovich S, Zimney EJ, et al. Preparation and characterization of graphene oxide paper. *Nature*. 2007;448:457–460.
2. Allen MJ, Tung VC, Kaner RB. Honeycomb carbon: a review of graphene. *Chem Rev*. 2010;110:132–145. doi:10.1021/cr900070d
3. Novoselov KS, Geim AK, Morozov SV, et al. Electric field effect in atomically thin carbon films. *Science*. 2004;306:666–669. doi:10.1126/science.306.5698.956a
4. Zhu SE, Yuan S, Janssen GCAM. Optical transmittance of multilayer graphene. *Europhys Lett*. 2014;108:17007. doi:10.1209/0295-5075/108/17007
5. Chiu NF, Huang TY. Sensitivity and kinetic analysis of graphene oxide-based surface plasmon resonance biosensors. *Sens Actuators B Chem*. 2014;197:35–42. doi:10.1016/j.snb.2014.02.033
6. Chung C, Kim YK, Shin D, et al. Biomedical applications of graphene and graphene oxide. *Acc Chem Res*. 2013;46:2211–2224. doi:10.1021/ar300159f
7. Sanchez VC, Jachak A, Hurt RH, et al. Biological interactions of graphene-family nanomaterials: an interdisciplinary review. *Chem Res Toxicol*. 2012;25:15–34. doi:10.1021/tx200339h
8. Bao Q, Loh KP. Graphene photonics, plasmonics, and broadband optoelectronic devices. *ACS Nano*. 2012;6:3677–3694. doi:10.1021/nn300989g
9. Johari P, Shenoy VB. Modulating optical properties of graphene oxide: role of prominent functional groups. *ACS Nano*. 2011;5:7640–7647. doi:10.1021/nn202666w
10. Chiu NF, Yang CD. Real-time and stepwise deoxidization processes to tune the photoluminescence properties of graphene oxide using EC-SPR spectroscopy. *RSC Adv*. 2018;8:11557–11565. doi:10.1039/C7RA13594G
11. Stebunov YV, Aftenieva OA, Arsenin AV, Volkov VS. Highly Sensitive and Selective Sensor Chips with Graphene-Oxide Linking Layer. *ACS Appl Mater Interfaces*. 2015;7:21727–21734. doi:10.1021/acsami.5b04427
12. Zhang H, Sun Y, Gao S, et al. A novel graphene oxide-based surface plasmon resonance biosensor for immunoassay. *Small*. 2013;9:2537–2540. doi:10.1002/smll.v9.15
13. Chiu NF, Huang TY, Lai HC, et al. Graphene oxide-based SPR biosensor chip for immunoassay applications. *Nanoscale Res Lett*. 2014;9:445. doi:10.1186/1556-276X-9-445
14. Chiu NF, Kuo CT, Lin TL, et al. Ultra-high sensitivity of the non-immunological affinity of graphene oxide-peptide-based surface plasmon resonance biosensors to detect human chorionic gonadotropin. *Biosens Bioelectron*. 2017;94:351–357. doi:10.1016/j.bios.2017.03.008
15. Chiu NF, Fan SY, Yang CD, et al. Carboxyl-functionalized graphene oxide composites as SPR biosensors with enhanced sensitivity for immunoaffinity detection. *Biosens Bioelectron*. 2017;89:370–376. doi:10.1016/j.bios.2016.06.073
16. Singh M, Holzinger M, Tabrizian M, et al. Noncovalently functionalized monolayer graphene for sensitivity enhancement of surface plasmon resonance immunosensors. *J Am Chem Soc*. 2015;137:2800−2803. doi:10.1021/ja511512m
17. Zagorodko O, Spadavecchia J, Serrano AY, et al. Highly sensitive detection of DNA hybridization on commercialized graphene-coated surface plasmon resonance interfaces. *Anal Chem*. 2014;86:11211–11216. doi:10.1021/ac502705n
18. Alwahib AA, Sadrolhosseini AR, An'amt MN, et al. Reduced graphene oxide/maghemite nanocomposite for detection of hydrocarbon vapor using surface plasmon resonance. *IEEE Photon J*. 2016;8:1−9. doi:10.1109/JPHOT.2016.2577592
19. Chiu NF, Yang CD, Chen CC, et al. Stepwise control of reduction of graphene oxide and quantitative real-time evaluation of residual oxygen content using EC-SPR for a label-free electrochemical immunosensor. *Sens Actuators B Chem*. 2018;258:981–990. doi:10.1016/j.snb.2017.11.187
20. Chiu NF, Chen CC, Yang CD, et al. Enhanced plasmonic biosensors of hybrid gold nanoparticle-graphene oxide-based label-free immunoassay. *Nanoscale Res Lett*. 2018;13:152–162. doi:10.1186/s11671-018-2565-7
21. Chiu NF, Lin TL. Affinity capture surface carboxyl-functionalized MoS2 sheets to enhance the sensitivity of surface plasmon resonance immunosensors. *Talanta*. 2018;185:174–181. doi:10.1016/j.talanta.2018.03.073
22. Lu YF, Lo ST, Lin JC, et al. Nitrogen-doped graphene sheets grown by chemical vapor deposition: synthesis and influence of nitrogen Impurities on carrier transport. *ACS Nano*. 2013;7:6522–6532. doi:10.1021/nn305697q
23. Teng CY, Yeh TF, Lin KI, et al. Synthesis of graphene oxide dots for excitation-wavelength independent photoluminescence at high quantum yields. *J Mater Chem C*. 2015;3:4553–4562. doi:10.1039/C5TC00492F
24. Zhang Y, Yuan S, Zhao Y, et al. Synthesis of novel yttrium-doped graphene oxide nanocomposite for dye removal. *J Mater Chem A*. 2014;2:7897–7903. doi:10.1039/C4TA01057D
25. Wang Y, Shao Y, Matson DW, et al. Nitrogen-doped graphene and its application in electrochemical biosensing. *ACS Nano*. 2010;4:1790–1798. doi:10.1021/nn100315s
26. Carnazza S, Foti C, Gioffre G, et al. Specific and selective probes for Pseudomonas aeruginosa from phage-displayed random peptide libraries. *Biosens Bioelectron*. 2008;23:1137–1144. doi:10.1016/j.bios.2007.11.001
27. Yao F, Zhang R, Tian H, et al. Studies on the interactions of copper and zinc ions with β-amyloid peptides by a surface plasmon resonance biosensor. *Int J Mol Sci*. 2012;13:11832–11843. doi:10.3390/ijms130911832
28. Chen H, Jia S, Zhang J, et al. Sensitive detection of copper(II) ions based on the conformational change of peptides by surface plasmon resonance spectroscopy. *Anal Methods*. 2015;7:8942–8946. doi:10.1039/C5AY02047F
29. Etayash H, Jiang K, Azmi S, et al. Real-time detection of breast cancer cells using peptide-functionalized microcantilever arrays. *Sci Rep*. 2015;5:13967. doi:10.1038/srep13967
30. Dudak FC, Boyaci IH. Peptide-based surface plasmon resonance biosensor for detection of staphylococcal enterotoxin B. *Food Anal Method*. 2014;7:506–511. doi:10.1007/s12161-013-9739-9
31. Tadepalli S, Kuang Z, Jiang Q, et al. Peptide functionalized gold nanorods for the sensitive detection of a cardiac biomarker using plasmonic paper devices. *Sci Rep*. 2015;5:16206. doi:10.1038/srep16206
32. Lim SK, Chen P, Lee FL, et al. Peptide-assembled graphene oxide as a fluorescent turn-on sensor for lipopolysaccharide (Endotoxin) detection. *Anal Chem*. 2015;87:9408–9412. doi:10.1021/acs.analchem.5b02270
33. Liang P, Li Q, Wu Z, et al. Graphene oxide-peptide nanoassembly as a general approach for monitoring the activity of histone deacetylases. *Analyst*. 2016;141:3989–3992. doi:10.1039/C6AN00902F
34. Kanchanapally R, Nellore BPV, Sinha SS, et al. Antimicrobial peptide-conjugated graphene oxide membrane for efficient removal and effective killing of multiple drug resistant bacteria. *RSC Adv*. 2015;5:18881–18887. doi:10.1039/C4RA14244F
35. Guo Y, Xu H, Li Y, et al. Hyaluronic acid and Arg-Gly-Asp peptide modified graphene oxide with dual receptor-targeting function for cancer therapy. *J Biomater Appl*. 2017;32:54–65. doi:10.1177/0885328217708638
36. Murray H, Baakdah H, Bardell T, et al. Diagnosis and treatment of ectopic pregnancy. *CMAJ*. 2005;173:905–912. doi:10.1503/cmaj.050222

37. Devaseelan P, Fogarty PP, Regan L. Human chorionic gonadotrophin for threatened miscarriage. *Cochrane Database Syst Rev*. 2010;5:CD007422.
38. Haddad B, Abirached F, Louis-Sylvestre C, et al. Predictive value of early human chorionic gonadotrophin serum profiles for fetal growth retardation. *Hum Reprod*. 1999;14:2872–2875. doi:10.1093/humrep/14.7.1722
39. Hoshi S, Suzuki KI, Ishidoya S, et al. Significance of simultaneous determination of serum human chorionic gonadotropin (hCG) and hCG-β in testicular tumor patients. *Int J Urol*. 2000;7:218–223. doi:10.1046/j.1442-2042.2000.00181.x
40. Ding X, Yang KL. Antibody-free detection of human chorionic gonadotropin by use of liquid crystals. *Anal Chem*. 2013;85:10710−10716. doi:10.1021/ac400732n
41. Chang CC, Chen CP, Lee CH, et al. Colorimetric detection of human chorionic gonadotropin using catalytic gold nanoparticles and a peptide aptamer. *Chem Commun*. 2014;50:14443–14446. doi:10.1039/C4CC06366J
42. Xia N, Chen Z, Liu Y, et al. Peptide aptamer-based biosensor for the detection of human chorionic gonadotropin by converting silver nanoparticles-based colorimetric assay into sensitive electrochemical analysis. *Sens Actuators B Chem*. 2017;243:784–791. doi:10.1016/j.snb.2016.12.066
43. Sun X, Liu Z, Welsher K, et al. Nano-graphene oxide for cellular imaging and drug delivery. *Nano Res*. 2008;1:203−212. doi:10.1007/s12274-008-8021-8
44. Chiu NF, Lin TL, Kuo CT. Highly sensitive carboxyl-graphene oxide-based surface plasmon resonance immunosensor for the detection of lung cancer for cytokeratin 19 biomarker in human plasma. *Sens Actuators B Chem*. 2018;265:264–272.
45. Compton OC, Jain B, Dikin DA, et al. Chemically active reduced graphene oxide with tunable C/O ratios. *ACS Nano*. 2011;5:4380–4391. doi:10.1021/nn202666w
46. Xue T, Cui X, Chen J, et al. A switch of the oxidation state of graphene oxide on a surface plasmon resonance chip. *ACS Appl Mater Inter*. 2013;5:2096–2103. doi:10.1021/am400481t
47. Okhrimenko DV, Nissenbaum J, Andersson MP, et al. Energies of the adsorption of functional groups to calcium carbonate polymorphs: the importance of −OH and −COOH groups. *Langmuir*. 2013;29:11062–11073. doi:10.1021/la402305x
48. Sousa M, Martins CHZ, Franqui LS, et al. Covalent functionalization of graphene oxide with D-mannose: evaluating the hemolytic effect and protein corona formation. *J Mater Chem B*. 2018;6:2803–2812. doi:10.1039/C7TB02997G
49. Stevens JS, Luca AC, Pelendritis M. Quantitative analysis of complex amino acids and RGD peptides by X-ray photoelectron spectroscopy (XPS). *Surf Interface Anal*. 2013;45:1238–1246. doi:10.1002/sia.5261
50. Brownson DAC, Kampouris DK, Banks CE. Graphene electrochemistry: fundamental concepts through to prominent applications. *Chem Soc Rev*. 2012;41:6944–6976. doi:10.1039/c2cs35105f
51. Karuppiah C, Cheemalapati S, Chen SM, et al. Carboxyl-functionalized graphene oxide-modified electrode for the electrochemical determination of nonsteroidal anti-inflammatory drug diclofenac. *Ionics*. 2015;21:231–238. doi:10.1007/s11581-014-1161-9
52. Imani R, Emami SH, Faghihi S. Nano-graphene oxide carboxylation for efficient bioconjugation applications: a quantitative optimization approach. *J Nanopart Res*. 2015;17:88–102. doi:10.1007/s11051-015-2888-6
53. Zhu Y, Li Z, Hao Z, et al. Optical conductivity-based ultrasensitive mid-infrared biosensing on a hybrid metasurface. *Light Sci Appl*. 2018;7:67–77. doi:10.1038/s41377-018-0066-1
54. Mohanty G, Sahoo BK. III-V nitrides and performance of graphene on copper plasmonic biosensor. *Superlattice Microst*. 2016;93:226–233. doi:10.1016/j.spmi.2016.03.040
55. Wu C, Rehman F, Li J, et al. Real-time evaluation of liver cancer cells by an in situ surface plasmon resonance and electrochemical study. *ACS Appl Mater Inter*. 2015;7:24848–24854. doi:10.1021/acsami.5b08066
56. Wang S, Boussaad S, Wang S, et al. High-sensitivity stark spectroscopy obtained by surface plasmon resonance measurement. *Anal Chem*. 2000;72:4003–4008. doi:10.1021/ac000504f
57. Zagorodko O, Bouckaert J, Dumych T. Surface plasmon resonance (SPR) for the evaluation of shear-force-dependent bacterial adhesion. *Biosensors*. 2015;5:276–287. doi:10.3390/bios5020276
58. Tassa C, Duffner JL, Lewis TA. Binding affinity and kinetic analysis of targeted small molecule-modified nanoparticles. *Bioconjug Chem*. 2010;21:14–19. doi:10.1021/bc900438a
59. Tang Y, Mernaugh R, Zeng X. Nonregeneration protocol for surface plasmon resonance: study of high-affinity interaction with high-density biosensors. *Anal Chem*. 2006;78:1841–1848. doi:10.1021/ac051868g